CyNET- a network analysis framework for high dimensionality, system level analyses of the functional Immunome.

Pavanish Kumar[1,2*], Joo Guan Yeo[1,2], Su Li Poh[1], Sharifah Nur Hazirah[1], Nursyuhadah Binte Sutamam[1], WX Gladys Ang[1], Vasuki Ranjani Chellamuthu[1], Martin Wasser[1], Jing Yao Leong[1], Lakshmi Ramakrishna[1], Thaschawee Arkachaisri[2,3], Salvatore Albani [1,2].

Affiliations :

[1]Translational Immunology Institute, SingHealth/Duke-NUS Academic Medical Centre, Singapore,

[2] Paediatrics Academic Clinical Programme, KK Women's and Children's Hospital,

[3] Duke-NUS Medical School and Rheumatology and Immunology Service, KK Women's and Children's Hospital, Singapore

* Correspondence: pavanish@nus.edu.sg

Abstract:

The immune system is a complex "Network of Networks", in which various immune cell subsets interact and influence each other's functions, ultimately determining immune competence and the control or onset of disease. The coordinated interactions between these cell subsets determine whether the outcome is a normal physiological state or a pathological condition. Established statistical procedures largely ignore the interactions between subsets and rely on statistically significant changes in the frequency of cell subsets. We developed CyNET (**Cy**tometry **Net**work)— an analysis platform based on a network science approach to understand the immune system holistically. CyNET enables us to quantify the systems level and subsets level properties. We show that changes in the centrality of the nodes (immune subsets) reflect better biological functions than changes in frequency. We used CyNET to analyze the immune development along the chronological age gradient. Peripheral blood cells from healthy newborns (cord blood), adults (20 to 55 years), and elderly (70 years and above) human subjects were further used for validation using single-cell transcriptomics. We found that network edge density, degree centralization, and assortativity score reflect the maturation and development of the immune system along the age axis, thus enabling the characterisation of the functional architecture of the Immunome and the identification of key functional hubs within the immune networks.

Introduction

High dimensionality approaches, in particular single cell proteomics using Mass Cytometry (CyTOF) and multiparametric fluorescent activated cell sorting (FACS) to include a larger number of markers available for staining, have contributed immensely towards our understanding of the immunome as a network of networks. High-dimensional cytometry has its challenges and requires innovative data-driven machine-learning (ML) approaches to understand the data generated. For example, a typical flow cytometry analysis requires biaxial plots and existing knowledge/hypothesis-driven sequential gating to characterize cell types. A test with just 30 markers requires 870 bi-axial plots and one with 40 markers will require 1560 bi-axial plots. It is therefore very challenging or probably impossible for humans to conceive and visualize over 1000 biaxial plots together to make sense of it, thus preventing the discovery of unexpected combinations of protein expression on a cell type and, most importantly, limiting the ability to understand the true architecture of the immunome, and the relevance of interactions among functionally relevant subsets. This need inspired an interdisciplinary collaboration between data scientists, ML scientists, and immunologists, thereby sparking a novel way of looking at these complex cytometric data. ML methods in concert with immunology expertise can lead to the development of approaches, that allow unbiased characterization and discovery of immune cell types and functions. Newer visualization methods (1-3) allowed a holistic understanding of the immune system. These developments are particularly relevant for clinical and translational research, and have sparked new approaches for data-driven theragnostics tools for precision medicine (4-6) and clinical development (7,8)

However, approaches that consider the relationship among the components of the immune response at system levels are still lacking. In real *in-vivo* conditions, various immune cell subsets interact and influence each other's functions. The coordinated interactions between these immune cell subsets eventually determine the outcome, reflected as a normal physiological state or pathological condition. Established statistical procedures used in cytometry analyses ignore the interactions between subsets and rely entirely on statistically significant changes in the frequency or percentage of cell subsets.

57 Also, no previous method has explored the understanding of the Immunome at a systems level yet,
58 and no measures have been investigated and developed to understand the properties of the system.
59 We have explored the core idea of Systems Immunomics (SI) in previous work while studying an
60 array of human diseases (9,8,10,11). In the present study, we developed the core idea further and
61 created a web application software named CyNET to facilitate the availability of an SI approach to
62 the broader community of immunologists and clinician scientists. We tested our approach by
63 analysing the immunome of healthy individuals from newborn (cord blood), adult (20 to 55 years),
64 and elderly (70 years and above) human subjects using CyNET. We further performed single-cell
65 transcriptomics analysis to validate the findings from CyNET network analysis. We propose here the
66 concept that centrality of given immune cell subsets within the network may be functionally relevant,
67 and integrates the use of frequency as the only parameter employed for a comprehensive
68 understanding of the immunone in health and disease.

69 **Results:**

70 **Network analysis framework:**

71 To understand the healthy immunome, we analyzed peripheral blood mononuclear cells (PBMCs)
72 using CyTOF. The data was obtained from the EPIC study (5). The samples from CBNB (newborn
73 cord blood, n=17), adult (25-55 years, n=17), and elderly human subjects (70 years and above, n=17)
74 were analyzed using CyNET software (see Methods). The analyzed data included PBMCs stained
75 with two CyTOF panels. Panel 1 (P1) was focused on T and NK cells, utilising PMA/ionomycin
76 stimulation to facilitate the identification of chemokine and cytokine-secreting cells, while Panel 2
77 (P2) was focused on detection of unstimulated monocytes/DCs and B cells. P1 and P2 data for the 3
78 age groups were analyzed using the EPIC analytics platform. Briefly, data was batch-normalized and
79 clustered into 100 subsets. The frequencies of the subsets were calculated for correlation network
80 analysis using CyNET. Subset phenotypes were identified using median marker intensity (Fig.S1).
81 The frequency of T and NK cell subsets from P1, B cells, and monocytes/DC subsets from P2 were
82 then used to build the immune cell network (Fig1). Immune cell clusters formed the nodes of the

network and to establish edge/connection between the clusters correlation coefficients >= 0.6 and p val < 0.05 were used. The network was visualized using force-directed layout algorithms from the igraph and visNetwork R packages. Each immune cell network's various system-level properties were calculated (Table 1). To calculate the network's modularity, the clusters were grouped into major lineage types as shown in Fig.1. Strong correlations between the subsets reflect potential direct or indirect interaction between the subsets.

Node Degree centrality reflects the changes in biological function, in some cases better than the frequency.

Communication hubs within the network are often pivotal for the appropriate functionality of the entire immunome. Thus, identifying the functional hubs and mechanistic drivers and how they relate to each other within the immunome is essential to understand its functionality. Here, we used Degree of Centrality (DC) to measure and identify the communication hub and drivers of immune homeostasis. We hypothesized that nodes with higher frequency, which denote higher abundance immune subsets, are functionally more important and may have higher interactions with other subsets. To our surprise, we observed that nodes with higher frequency do not always show a higher DC. The correlation analysis between the median frequency and DC showed no significant correlation in either CBNB (r=0.099, p=0.391), adult (r= 0.151, p=0.121) or elderly (r=0.026, p=0.802) group (Fig.1A). Consequently, we systematically investigated the immune cell subset properties for the major cell lineage groups.

T cells: There were 43 CD4 T cell subset nodes (Fig. S2A), which accounted for maximum edges in all three networks (Fig.S3). CD4 T cell subsets formed the majority of cells in CBNB (median = 60 %) while in adults (41%) and elderly (44%) it was lower than CBNB (Fig.S4). Among the 43 CD4 T cell nodes only a few were more enriched in CBNB than in adult and elderly subjects (Fig. S2A). These more abundant CD4T cell nodes from CBNB (Nodes 1, 2,25,34,44,73) expressed CD45RA, a naive T cell marker, explaining their lower interactions and the lesser DC(Fig.2B).

108 In contrast, memory CD4T cell (CD45RO+) subsets (Nodes 18, 27, 30,41,6) showed a higher DC
109 than the CD45RA+ nodes (Fig.2A). We investigated the phenotype of the most central CD4 T cell
110 node (Node10). Node10 showed a phenotype (CXCR5+PD1+) of Tfh (T follicular helper cells)
111 (Fig.S1A). This Tfh subset had the highest DC (DC = 22) in the adult network while in CBNB
112 (DC=2) and elderly (DC =1) immune cell networks its DC was much lower (Fig.2B). Similarly, a
113 Th17 subset (Node 29) had lower frequency in all three groups compared with many other CD4 T
114 cell nodes, however this node (Node 29) showed higher DC in adults' network (Fig.2B). Although,
115 CBNB samples had the highest fraction of CD4 T cells, heterogeneity was reduced, when compared
116 to adult and elderly, where many nodes were present with similar frequency. The average DC of the
117 CD4 T cell node in CBNB was lower (average DC = 2.35) compared to adult (average DC = 5.2) and
118 elderly (average DC = 4.3).
119 Similar to CD4 T cell subsets, CD8 T cell subsets from CBNB showed a lower degree of centrality
120 for the subsets (Node 76, 65,66,56,57,45) with higher median frequency (Fig.2C). These CBNB
121 enriched CD8 T cell subsets expressed IL10 and FOXP3, suggesting a regulatory phenotype
122 (12,13,14) which may play a role in tolerance induction. Furthermore, the most abundant CD8 subset
123 (Node67) in the elderly showed 0 DC, and another abundant subset Node69 also showed lower DC
124 (DC = 6) (Fig. 2C), conversely Node 63 showed the highest DC (DC = 15) even though its median
125 frequency was much lower (median frequency < 0.01) (Fig. S2C). Node67 and Node69 had an
126 exhausted phenotype (CD28- CD45RA+), and Node63, except for CD3 and CD8, was negative for
127 most markers that we analysed (Fig.S1A).
128 **Innate cells (NK, DC):** A total of 8 NK cell subsets were identified (Fig. S2C). The NK cell subsets
129 showed lower DC in adult than in elderly subjects' network (Fig. S2C). In CBNB, both frequency
130 and degree of centrality were low (Fig. S2C). The most abundant NK subset (Node89) in the elderly
131 was of a CD161+ GZMB+IFNg-low phenotype the while the subset with the highest DC (Node87)
132 was CD161-GZMB+IFNg+ (Fig.2D, Fig.S1).

133 In CBNB, the most abundant monocyte subset (Node76) was HLA-DR negative and CD86 low, in
134 contrast, the most frequent subset (Node86) in adults and the elderly was HLA-DR and CD86
135 positive. Here again, the DC of the most monocyte subsets in CBNB was lower compared to adult
136 and the elderly (Fig.3A). Most abundant subsets (Node 65,66,76,96) in CBNB were negative for
137 HLA-DR expression. HLA-DR is required for antigen presentation to T cells, and a lack of it on
138 CBNB monocytes shows impairment or lack of cellular function by monocytes. Interestingly, the
139 proportion of edges between monocyte subsets (12.1%) was highest in CBNB even though the CBNB
140 network was sparse while the converse is true for adults' immune cell network with the lowest edge
141 fraction between the monocytes (5.4%) (Fig.S3). In the adult immune network, monocytes were
142 connected to many subsets of other lineages, while in CBNB the monocytes were mostly connected
143 to other monocyte subsets (Fig1).
144 **B cells**: The major function of B cells is the production of neutralizing antibodies against invading
145 pathogens. B cell subsets were low in CBNB and elderly subjects compared to adults (Fig.S4). In
146 CBNB, only subset (Node79) which had a phenotype (CD19+CD38+CD24+IL10+) consistent with
147 regulatory B cells (Breg) (Fig.S1B) showed DC greater than 5 and it was not the most abundant subset
148 in the CBNB(Fig.3B). Breg cells are involved in the early maintenance of pregnancy and thus may
149 have functional importance in the developing fetus. In adults, a naive B cell subset (Node60) showed
150 the highest degree centrality (Fig.3B). This subset also expressed trafficking receptor CXCR4 and
151 low levels of plasmocytoid dendritic cell (pDC) specific receptor CD303. Both, B cells and pDC can
152 be generated from common lymphoid precursors (CLP) and low levels of CD303 on naive cells may
153 suggest that this subset is at earlier end of the maturation state. In the elderly immune network, B cell
154 subsets showed edges between themselves and clustered as isolated module (Fig.1C). The isolated
155 cluster of B cells suggests a loss of B cell cross talk/engagement in the overall immune cell network
156 with aging.
157

158 **Network edge density, and centralization score reflect the maturation and development of the**
159 **immune system along the age gradient**

160 Tools to understand and dissect immune functions and their relations at systems level have not been
161 developed yet. In the present study we investigated how the various elements of the Immunome
162 interlace functionally, and hypothesise that these interactions affect the function and phenotype of
163 individual immune functions within the network. In particular, we investigated graph density,
164 centralisation score, assortativity score and modularity as a relevant attribute to understand and depict
165 the development and maturation of the immune system with age.

166 The graph or edge density of the network is the ratio of edges observed to maximum possible edges
167 in the network. The edge density of a network ranges from 0, for a completely isolated network, to 1
168 for a completely connected network, and is a measure of overall interaction in the network. We
169 hypothesized that the developing, immature immune cell subsets in CBNB will have a lower network
170 edge density compared to adults and elderly immune cell networks. As expected, we found that the
171 edge density was lowest for CBNB (0.0257) compared to network densities of the adult (0.0578) and
172 elderly (0.0521) (Table 1). Lower edge density was also visually apparent in the CBNB network,
173 where many nodes were isolated and had no edges between them (Fig.1A). Also, we found that the
174 total number of edges (total edges = 149) in the CBNB network was lower than the network of adult
175 (total edges = 335) and elderly (total edges = 301) human subjects. Moreover, the percentage of
176 negatively correlated edges was higher in CBNB (37.5%) than in adults (21.7%) and elderly (12.6%)
177 networks. The decrease in negatively correlated edges suggests a loss of counterbalancing regulatory
178 and inhibitory functions of the network. These data provide another perspective to the notion that
179 aged/elderly populations are more prone to pro-inflammatory conditions than younger and adult
180 individuals.

181 We further analyzed the centralization score, which measures the importance and dominance of the
182 nodes in the network. A centralization score of 0 means all nodes in the network are equally central
183 or equally important, while a centralization score of 1 suggests only 1 node completely dominates the

network. Intuitively, we hypothesized that at the earlier stages of development, immune cell networks are less centralised as specialized functions of the cells may not have emerged or developed yet, and with development and antigen experience more nodes will take a specialised role and thus will dominate the network or subnetworks. This will be reflected as higher centralization of the network. We quantified the degree centralization score of the CBNB (0.105), adult (0.148), and elderly (0.154) immune cell network, and observed an increase in the centralization score on the age axis. We also observed a concordant pattern in graph degree assortativity, which is another measure for preferential attachment between hub or highly connected network nodes(15), with an increase in degree assortativity score on the age axis (Table 1). Thus, the development of cells and exposure to stimuli with increasing age lead to the development of more specialized immune cell subsets with an increased ability to interact with other subsets, reflected as an increase in the preferential attachment or assortativity score of the network.

We also hypothesized that age would affect the modularity of immune networks. Modularity reflects inter and intra-communication of the node members within the network, where interactions within the same community increase the modularity score while interactions between communities lower the modularity. In our immune cell networks, major cell lineages were delineated as communities for modularity score calculation. We observed that modularity increased along the age axis (Table 1), indicating loss of communication between the major cell lineage subsets with age. Within this context, B cell subsets formed an isolated cluster in the elderly immune, in comparison with the higher number of inter-subset interaction of B cells in adult immune network (Fig.1). While the total B cell edges in the adult and elderly networks were 30 and 32, respectively., 36 % (11 edges) were solely between the B cell subsets in the adult network while this was much higher 56% (18 edges) in the elderly network (Fig.S3). Similarly, intra-subset edges within the monocyte/DC subsets increased from adult (19%) to elderly (28%). Overall, the immune network of CBNB was sparse, with much lower modularity than adult and elderly.

210 **Single-cell Transcriptomics analysis:**

211 As Ligand and Receptor (LR) interactions between cells comprise of the most common ways of cell-
212 cell communication, we hypothesized that interactions inferred from the correlation network could
213 be explained by LR interaction between the cell subsets. More connected nodes, as reflected in a
214 higher degree centrality score, would thus have higher LR interaction potential with other subsets.
215 Thus, to validate the correlational structure and degree centrality of a subset we performed LR
216 interaction analysis between immune cell subsets from PBMCs using single-cell RNA sequencing
217 (scRNA-seq). We performed 10x drop-seq based scRNA-seq on PBMCs from CBNB(n=5),
218 adult(n=6), and elderly(n=4) human subjects (Table S1). After QC and filtering 22975 cells were
219 retained for analysis (see Methods). scRNA-seq data was batch corrected using the SCT transform
220 method, and transformed data was used for predicting the expression of genes using the ALRA zero
221 count preserving algorithm(16). The ALRA predicted gene count matrix was then used for cell type
222 identification. The SingleR package was used for cell type identification using immune cell signature
223 from MonacoImmuneData from celldex R package(17). A total of 25 cell types were identified (Fig.4,
224 Table S2) using scRNAseq. The most abundant cell types recovered in CBNB and adults were naive
225 CD4 T cells while in the elderly NK cells were most abundant. In our immune network analysis naive
226 CD4 T cells have lower interaction across all age groups compared to other CD4 T cell subsets such
227 as Th17, Tfh and Tregs (Fig.2A). In agreement with these observations, differential LR gene
228 expression analysis between naive CD4 T cells and the rest of CD4 T cells showed lower expression
229 of 57 LR genes and higher expression of 41 LR genes in naive CD4T cells (Table S3). The low
230 expressed genes included the key LR genes such as chemokines and cytokines receptors (*CCR4,*
231 *CCR6, CCR10, CXCR3, IL10RA, IL17RB, IL2RA, TNFRSF1B*), chemokine, cytokine (*CCL5, IL2*)
232 and integrin (*ITGB1, ITGAV, ITGA2*) genes. Among the highly expressed LR genes were growth
233 factors such as *FLT1*, and *IGF1R*. Inhibitory receptors such as *PECAM-1* and *BTLA* were also more
234 expressed in naive CD4T cells. The dampening of key chemokines/cytokines, chemokine/cytokine
235 receptors, and integrin genes explains the lower interaction of naive CD4T cells with other immune

236 cells. The CBNB immune cell network was the most sparse with lower interactions between subsets
237 (Fig.1A). Both CyTOF (Fig.S4) and scRNA-seq data (Fig.4) showed naive CD4 T cells as the most
238 abundant immune cells in CBNB group.

239 **KLRB1+ NK cell subset is more central in the elderly group immune cell network.**

240 A higher degree of centrality is an indication of more inter-cellular interactions. Accordingly, we
241 hypothesized that the higher degree of centrality will be reflected as higher LR interaction among the
242 subsets. First, we performed t-SNE based dimensionality reduction and clustering for NK cell subsets.
243 Total NK cells (n=4595) from 3 groups clustered into 12 clusters, using lovian clustering algorithm
244 (Fig.5A). Distribution of NK cells on t-SNE plots suggested unique NK cell profile in CBNB, adult,
245 and elderly subjects (Fig.5B). CyTOF data showed, lower frequency (Fig.S4) and degree centrality
246 (Fig.2C, Fig.S2C) for NK cells clusters in CBNB and adult. The two NK subsets (Node87 and
247 Node89) in the elderly immune cell network were unique for its highest degree of centrality and
248 frequency (Fig.5D, Fig. 2C) respectively. These subsets were different in their CD161 expression
249 (Fig.S1A). Node87 expressed CD161 while Node89 was negative for CD161 surface expression. To
250 mirror the CyTOF NK cell phenotype we looked at *KLRB1* (which encodes CD161) gene expression
251 in NK cell clusters from scRNA-seq transcriptomics analysis (Fig.5C). In adults, the majority of cells
252 in clusters 1,4 and 9 were *KLRB1* positive, while in elderly subjects' *KLRB1* high subsets were in
253 clusters 0 and 2(Fig.5C). We compared the LR interactions between *KLRB1* negative (cluster 3 =
254 NK_3) and *KLRB1* positive (cluster 0 = NK_0) NK cell clusters in elderly subject to mirror the cell
255 phenotype of the Node89 (CD161-) and Node87 (CD161+) subsets from the CyTOF data (Fig.5D).
256 Significantly enriched LR pairs between the NK_0 or NK_3 and all other subsets were obtained using
257 CellChat (18). LR pairs common to both NK_0 and NK_3 were removed and only LR specifically
258 enriched in either NK_0 or NK_3 were counted to understand the interaction potential specific for
259 the *KLRB1* negative and KLRB1 positive NK cell subset. The total LR pair numbers between any
260 subset and NK_0 (*KLRB1*+) were higher than for the NK_3 (*KLRB1*-) subset (Fig.5E). When we

261 analyzed the LR pair directionally, we observed that there were more ligand signals from the NK
262 subset (Fig. S5A) then ligand signal to the NK cell subsets (Fig.S5B).
263 Hence, higher LR interaction between *KLRB1*+ NK cells with other immune cell subsets corroborates
264 the higher degree centrality and interaction of CD161+ NK cells in the elderly immune cell network.
265 **Lower LR interactions of CD28- CD8T cells explain exhaustion and immune aging**
266 An increase in CD28- CD8+ senescent and dysfunctional T cells in the elderly population is widely
267 reported(19). CyTOF data in our study recapitulates this observation. CD28-CD8 T cells (Node
268 69,67) were more abundant than CD28+ CD8T cells in the elderly population, however, CD28- CD8T
269 subset's degree centrality was lower (Fig.2B). We contrasted LR interactome analysis for CD28-
270 CD8T with CD28+CD8T cells to understand potential differences in inter-subset communication.
271 To perform LR interaction analysis for CD8 T cells, we pooled all CD8T cells (CD8_ Naive,
272 CD8_EM, CD8_CM, CD8_TE) and reclustered them and performed t-SNE dimensionality reduction
273 for visualisation. We obtained 6 clusters (Fig.6A). Among a total of 2294 CD8 T cells ,1942 were
274 naive CD8 T cells and 253 were terminally exhausted CD8 T cells. Comparatively, central
275 memory(n=21) and effector memory (n=78) T cells were much lower in numbers (Fig.6B).
276 We tested the LR interactions in *CD28*- and *CD28*+ CD8T cell clusters from adult and CBNB (Fig.6)
277 in scRNA-seq data. In the elderly subject group, we obtained a very low CD8 T cell count (n=100)
278 (Fig.6C). *CD28*+ cluster in adult (CD8_1) was compared with *CD28*- cluster (CD8_2), similarly,
279 CD8_5(*CD28*+) cluster was compared with CD8_0 (*CD28*-) cluster in CBNB. We observed lower
280 LR interaction enriched in *CD28*- CD8 T cells compared to *CD28*+ T cells (Fig.6E, 6F). Lower
281 degree centrality and lower LR interaction of CD28- CD8T cells may thus be one explaintion for
282 exhaustion and loss in communication ability with other immune cell subsets within the immune
283 system.
284
285
286

287 **Discussion**

288 Immune cells do not function in isolation, but they interact and influence each other and these overall
289 interactions are ultimately reflected as a healthy or diseased phenotype. These cellular interactions
290 lead to a network structure that is specific to any given immune condition and function. Current
291 analysis approaches are mostly reductionist and siloed and fail to represent the complexity of the
292 immune system in health and disease. To the best of our knowledge, no measures were ever used or
293 reported to understand the overall immune cell network in a relational, high dimensionality fashion.
294 Here, we developed a novel systems immunology analytic approach and have created a web
295 application software, CyNET, for high dimensional cytometry data analysis. Our analysis approach
296 nested in CyNET allows an understanding of the immune response holistically at the systems level.
297 We proposed and have validated degree of centrality as an efficient measure of function, which
298 complements the mere calculation of frequency of the immune cell subsets. We developed various
299 systems level measures that capture the relevant biological phenotype. CyNET allows inference of
300 cellular interaction among immune subsets and subnetworks. scRNA sequencing and LR based
301 interactome analysis further validated our inference from the CyNET immune cell network.

302 We investigated systems level properties such as network density, centralization, and assortativity, to
303 quantify the immune response at the network level(20). We measured these properties in the context
304 of the development of the immune system with age, taking advantage of an already existing, highly
305 curated cytometry dataset (5,11,21). The lifecycle of the immune system starts with the development
306 of a child in the mother's womb and continues throughout the individual's life span. Immune cells at
307 birth are immature and start gaining lineage and functional maturity depending on the environmental
308 stimuli. With time, more immune cells gain exhausted characteristics leading to the aging of the
309 immune cells. This immune aging is not only observed in elderly human subjects but is also observed
310 in some autoimmune diseases at early ages. Immature cells during early age will have lower
311 functionality and lower interaction ability with other subsets, a characteristic, which we could capture
312 in our network density analyses. We showed both visually and quantitatively (Fig.1) that network

313 density is lowest in CBNB and highest in adults where cells are fully matured but not as exhausted
314 as in elderly subjects. Network centralization further captures the emergence or change of functional
315 units in the network. Immune cells mature to take up a more specialized function during development
316 or with exposure to antigens and external stimuli. With maturation, these specialized cells dominate
317 in the network in comparison to other subsets. This notion of increased dependence of the network
318 on a few subsets can be quantified using network centralization. As observed, an increase in network
319 centralization with age precisely captures the emergence of more specialized functions. At birth, the
320 majority of the cell subsets are in development and have not undergone enough antigen exposure,
321 thus the network is less centralised.
322 In contrast, immune cells in the elderly population have been exposed to external stimuli and
323 developed more specialized functions in response to such stimuli. Thus, in elderly populations, some
324 of the immune cells dominate, leading to a more centralised immune cell network. Maturation of the
325 immune cells will lead to preferential attachment of the nodes to generate immune response specific
326 to stimuli. This could be evaluated using assortativity degree of the network. Indeed, increase in
327 centralization score and assortativity degree along the age axis rightly captured the immune cell
328 maturation at the systems level in our study.
329 Network-level properties can be very useful for monitoring and understanding the system as a whole
330 unit. However, to understand the mechanisms and to optimally manipulate the system for therapeutic
331 development, the understanding of the key nodes within the system is required. Conventionally, in
332 disease vs control comparisons, changes in the frequency of hypothesized immune cell subsets are
333 evaluated to understand the mechanistic relevance of a given subset in health and disease. Here, we
334 propose instead that the centrality of subsets serve as a better measure to understand their functional
335 relevance in patho-physiological systems. For proof of concept, we investigated the change in
336 frequency and degree of centrality of the nodes in the network along the gradient of aging. The overall
337 degree of centrality of naive CD4T cell subsets was lower than other CD4T cell subsets such as Tfh
338 or Treg cells. Thus, higher percentage of naive CD4 T cells in CBNB results in a functionally

339 immature and developing immune system. Tfh frequency in adults and the elderly were similar.
340 However, the degree centrality of Tfh in adults was much higher than in the elderly population. The
341 centrality of Tfh suggested a loss of B cell and antibody secretion functionality in an elderly
342 population. It is well-known and reported that the elderly population is less efficient in generating
343 and maintaining a good antibody titer upon vaccination (22,23). B cells present antigens to Tfh cells
344 and successful engagement of B cells with Tfh protects B cells from death and promotes reentry into
345 the cell cycle. In the germinal center (GC) these B cells mature and exist as antibody producing
346 memory B cells. The loss of Tfh and B cell interactions may further lead to a reduction in B cells that
347 we also observed in an elderly population.
348 Furthermore, the B cell subsets in the elderly network (Fig.1C) was clustered as a module and were
349 more correlated with each other than with other lineage subsets. Conversely, in adults B cells were
350 more connected with other lineage subsets (Fig.1B). The lower Tfh degree centrality, lower B cell
351 fraction, and isolated module of B cell subsets in the elderly immune cell network accurately highlight
352 the loss of B cell functionality in the elderly population. Like Tfh, the proportion of Th17 (Node 29)
353 was similar in the adult and elderly populations. However, the degree centrality of Th17 subsets was
354 lower in the elderly than in the adult population. Our observation corroborates with a recent study
355 that suggests aging weakens the pathogenicity of Th17 cells (24).
356 One of the hallmarks of immune aging is the increase in CD28- CD8 T cell frequency(19). CD28 is
357 a costimulatory molecule and is required for successful T-cell activation when the TCR recognizes
358 its cognate antigen presented with MHC. In elderly subjects and autoimmune conditions, constant
359 antigenic exposure and repeated antigenic stimulation lead to loss of CD28 expression on CD8 T cells
360 (19). Low vaccination response in the elderly correlates with a high frequency of CD28- T cells.
361 CD28-CD8T cells negatively impact immune response through various mechanisms. Our study
362 further extends this knowledge and suggests reduced intra-cellular communication potential by
363 altered LR interactions render these cells anergic and dysfunctional in elderly subjects.

364 NK cell numbers rise with age and the expression of various surface markers on NK cells also changes
365 with age (25-27). We observed a similar increase in NK cell subsets in the elderly population. NK
366 cell expresses many inhibitory and activatory receptors and shows substantial heterogeneity. Among
367 the increased NK cell subsets in elderly group, CD161- subsets were more abundant than CD161+
368 subsets (Fig. 2C). Only one NK cell subset (Node 87) was positive for CD161 expression (Fig.S1A).
369 CD161 expression on NK cells marks responsiveness to pro-inflammatory cytokines, increased
370 expression of integrins, and tissue residency markers (28). CD161 expression is lost in CMV-induced
371 terminally differentiated NK cells (28). Human CMV-induced adaptive NK cell subset also shows
372 downregulation of CD161 gene expression, and these adaptive NK cells are suggested to have
373 emerged for immune-surveillance of infected cells with improved proliferation and survival capacity
374 in inflammatory conditions (29). The lower degree centrality, and LR interaction potential of the
375 CD161- NK cell subsets compared to CD161+ NK cell subsets corroborates and explains the
376 reduction in signaling proteins and response to proinflammatory cytokines by CD161- NK cells.
377 CD161+ NK cells are inhibitory and probably enable immune homeostasis and relative contraction
378 of these cytokine-responsive subsets in the elderly population may further add to immune aging.
379 Altogether, we have broadened our high dimensionality approach to the analysis of the Immunome
380 across the age gradient with an in depth understanding of the relational networks, which shape
381 mechanisms of immune responses and their evolution. Some of our findings show a surprising
382 discordance between frequency and centrality for given, mechanistically relevant, immune subsets,
383 thus underscoring the importance to integrate the traditional approach based on cell frequency in a
384 given subset with Network analyses capable to define the relational relevance of such subsets. We
385 offer here to the community (https://epicimmuneatlas.org/shiny/CyNET) the necessary tools and
386 dataset to apply this sort of analysis to various conditions, in the hopes of expanding and strengthening
387 this approach.
388
389

390 **Methods**:

391 **CyNET web application**: The CyNET web application was created using the R shiny web
392 framework. For network analyses igraph R package was used, and for network visualisation
393 visNetwork, and ggplot2 R packages were used.

394 **CyTOF data analysis**: CyTOF data for CBNB, adults and elderly subjects were downloaded from
395 EPIC (epicimmuneatlas.org). Data was clustered into 100 clusters for both Panel 1 and Panel 2
396 dataset. Cluster frequency and median marker expression data was downloaded and used for network
397 analysis. T cells and NK cells from Panel 1 data, B cells and Monocyte/DC data from Panel 2 data
398 set was merged together create a full lineage set data matrix. To balance the sample number in each
399 group 17 sample (Maximum number of samples available for elderly group in the dataset) from each
400 category was randomly taken for correlation network analysis. To create the correlation network
401 correlation (R2 = 0.5) and p-value (<0.05) cutoff was applied to establish a n edge between the nodes.
402 The immune cell clusters were the nodes of the network and the edges between them was considered
403 potential direct or indirect interaction. To create the network and calculate the network properties
404 igraph R package and custom R code was used. To visualise the network visNetwork R package was
405 used.

406 **Healthy Human blood sample collection:** Peripheral blood samples were collected from
407 CBNB(n=5), adult(n=6), and elderly(n=4) healthy human subjects. Subject's demographic
408 information is provided in Supplementary Table S1. Human subjects were recruited at KK
409 Women's and Children's Hospital, Singapore. The study was reviewed and approved by the
410 SingHealth Central Institutional Review Board. The Informed consent was obtained according to
411 the SingHealth Central Institutional Review Board (CIRB) requirements.

412 **Peripheral blood mononuclear cells (PBMCs) preparation:** Peripheral blood samples were
413 collected in ethylene diamine tetra acetic acid tubes (EDTA). PBMCs were isolated from blood
414 samples using Ficoll-Paque (GE Healthcare) gradient centrifugation within 6 hrs from recruitment,
415 and were stored in liquid nitrogen until further use.

416 **Single cell Library preparation and sequencing**: PBMCs were thawed and rested for 30 minutes.
417 Cells were washed with PBS twice and Single cells were encapsulated into droplets with a gel bead
418 in the emulsion (GEM) method using the 10x Chromium controller. The Chromium Single Cell 3'
419 gene expression protocol (version 3 chemistry,10x Genomics) was used. Downstream library
420 construction was performed using the 10x 3' Gene Expression Library Construction kit, and
421 barcoding was carried out with i7 Illumina adaptor indexes. Pooled libraries were then sequenced on
422 the Illumina HiSeq 4000 platform using paired-end 151-bp reads to achieve 50,000 reads per cell for
423 gene expression

424 **Single cell data analysis:**

425 Raw reads for transcriptomic analyses were aligned to the human genome (hg19- 3.0.0) using Cell
426 Ranger version 7 software. CellRanger's count utility was used to count the features. Cell barcodes
427 and feature count matrices were created by aggregating filtered feature counts of each sample using
428 the Cell Ranger aggregate utility. Subsequent data normalization and analysis were performed using
429 the Seurat R package and custom R code. Cell count data were quality controlled and filtered based
430 on cellular complexity (number of genes per cell) and mitochondrial reads. Cells with between 300
431 and 5,000 genes and mitochondrial percent reads less than 20 were kept for analysis. Data scaling,
432 normalization, variable gene identification and clustering were performed using the Seurat pipeline.
433 SCT transform method from Seurat R package was used for batch normalisation. Batch normalised
434 data was used for imputation of gene counts using ALRA algorithm (16). Imputed gene count
435 matrix was further used for cell type annotation using SingleR package and MonacoData set
436 signature. For clustering within the annotated subsets Lovian clustering was performed.

437 **Ligand Receptor analysis**: To find the potential interaction between immune cell subsets/clusters,
438 networks of clusters created based on enriched LR pairs between the clusters. CellChat package
439 (18) was used to find significantly enriched LR pairs between the immune subsets. For
440 visualisation and analysis visNetwork, ggplot2 and customs R code was used.

441

442 **Data availability**

443 The software application can be accessed on https://epicimmuneatlas.org/shiny/CyNET.

444 Raw RNA sequencing data are from human subjects and will be provided upon request in

445 alignment with institutional and grantor guidelines.

446 **Code availability**

447 Custom code will be given on reasonable request.

448 **Conflicts of interest disclosure**

449 The authors declare no conflicts of interest.

450 **Acknowledgement**

451 We thank all participants and their families who gave consent for samples. This study was

452 supported by grants from the NMRC (MOHIAFCAT2/005/2015, NMRC/OFLCG/002/2018,

453 CIRG19may0052), MOH-STaR19nov-0002, A*STAR PEC21-H22P0M0003, Duke-NUS and

454 SingHealth AMC core funding is gratefully acknowledged. This research is also supported by the

455 Singapore Ministry of Health's National Medical Research Council under its Centre Grant

456 Programme (MOH-000988)

457 **Author contributions**

458 P.K performed the experiments and bioinformatics analysis. S.L.P, S.N.H, N.B.S, V.R.C,

459 W.X.G.A, J.Y.L performed the experiments. J.G.Y and T.A. recruited the human subjects. T.A,

460 J.G.Y, L.R.K., W.X.G.A, M.W. participated in study design and manuscript preparation. P.K, and

461 S.A conceived and lead the study and wrote the manuscript. SA arranged funding for the study

Bibliography

1 Qiu, P. *et al.* Extracting a cellular hierarchy from high-dimensional cytometry data with SPADE. *Nat Biotechnol* **29**, 886-891 (2011). https://doi.org:10.1038/nbt.1991

2 Maaten, L. J. P. v. d. Accelerating t-SNE using Tree-Based Algorithms. *Journal of Machine Learning Research* **15**, 3221-3245 (2014).

3 Melville, L. M. a. J. H. a. J. UMAP: Uniform Manifold Approximation and Projection for Dimension Reduction. *arXiv*, 1802.03426 (2020).

4 Leong, J. Y. *et al.* Immunome perturbation is present in patients with juvenile idiopathic arthritis who are in remission and will relapse upon anti-TNFalpha withdrawal. *Ann Rheum Dis* **78**, 1712-1721 (2019). https://doi.org:10.1136/annrheumdis-2019-216059

5 Yeo, J. G. *et al.* The Extended Polydimensional Immunome Characterization (EPIC) web-based reference and discovery tool for cytometry data. *Nat Biotechnol* **38**, 679-684 (2020). https://doi.org:10.1038/s41587-020-0532-1

6 Mishra, A. *et al.* Microbial exposure during early human development primes fetal immune cells. *Cell* **184**, 3394-3409 e3320 (2021). https://doi.org:10.1016/j.cell.2021.04.039

7 Nguyen, P. H. D. *et al.* Trajectory of immune evasion and cancer progression in hepatocellular carcinoma. *Nat Commun* **13**, 1441 (2022). https://doi.org:10.1038/s41467-022-29122-w

8 Tan, T. J. *et al.* A phase I study of an adenoviral vector delivering a MUC1/CD40-ligand fusion protein in patients with advanced adenocarcinoma. *Nat Commun* **13**, 6453 (2022). https://doi.org:10.1038/s41467-022-33834-4

9 Kumar, P. *et al.* Pro-inflammatory, IL-17 pathways dominate the architecture of the immunome in pediatric refractory epilepsy. *JCI Insight* **5** (2019). https://doi.org:10.1172/jci.insight.126337

10 Paleja, B. *et al.* Systemic Sclerosis Perturbs the Architecture of the Immunome. *Front Immunol* **11**, 1602 (2020). https://doi.org:10.3389/fimmu.2020.01602

11 Kumar, P. *et al.* Pro-Inflammatory Derangement of the Immuno-Interactome in Heart Failure. *Front Immunol* **13**, 817514 (2022). https://doi.org:10.3389/fimmu.2022.817514

12 Joeris, T. *et al.* Intestinal cDC1 drive cross-tolerance to epithelial-derived antigen via induction of FoxP3(+)CD8(+) T(regs). *Sci Immunol* **6** (2021). https://doi.org:10.1126/sciimmunol.abd3774

13 Liston, A. & Aloulou, M. A fresh look at a neglected regulatory lineage: CD8(+)Foxp3(+) Regulatory T cells. *Immunol Lett* **247**, 22-26 (2022). https://doi.org:10.1016/j.imlet.2022.05.004

14 Niederlova, V., Tsyklauri, O., Chadimova, T. & Stepanek, O. CD8(+) Tregs revisited: A heterogeneous population with different phenotypes and properties. *Eur J Immunol* **51**, 512-530 (2021). https://doi.org:10.1002/eji.202048614

15 M.E.J.Newman. Assortative mixing in networks. *Phys. Rev. Lett.* **89** (2002). https://doi.org:https://doi.org/10.1103/PhysRevLett.89.208701

16 Linderman, G. C. *et al.* Zero-preserving imputation of single-cell RNA-seq data. *Nat Commun* **13**, 192 (2022). https://doi.org:10.1038/s41467-021-27729-z

17 Monaco, G. *et al.* RNA-Seq Signatures Normalized by mRNA Abundance Allow Absolute Deconvolution of Human Immune Cell Types. *Cell Rep* **26**, 1627-1640 e1627 (2019). https://doi.org:10.1016/j.celrep.2019.01.041

18 Jin, S. *et al.* Inference and analysis of cell-cell communication using CellChat. *Nat Commun* **12**, 1088 (2021). https://doi.org:10.1038/s41467-021-21246-9
19 Weng, N. P., Akbar, A. N. & Goronzy, J. CD28(-) T cells: their role in the age-associated decline of immune function. *Trends Immunol* **30**, 306-312 (2009). https://doi.org:10.1016/j.it.2009.03.013
20 Csardi, G., Nepusz, T. The igraph software package for complex network research. *InterJournal* **Complex Systems**, 1695 (2006).
21 Yeo, J. G. *et al.* A Virus-Specific Immune Rheostat in the Immunome of Patients Recovering From Mild COVID-19. *Front Immunol* **12**, 674279 (2021). https://doi.org:10.3389/fimmu.2021.674279
22 Collier, D. A. *et al.* Age-related immune response heterogeneity to SARS-CoV-2 vaccine BNT162b2. *Nature* **596**, 417-422 (2021). https://doi.org:10.1038/s41586-021-03739-1
23 Lee, J. L. & Linterman, M. A. Mechanisms underpinning poor antibody responses to vaccines in ageing. *Immunol Lett* **241**, 1-14 (2022). https://doi.org:10.1016/j.imlet.2021.11.001
24 Li, H. *et al.* Aging weakens Th17 cell pathogenicity and ameliorates experimental autoimmune uveitis in mice. *Protein Cell* **13**, 422-445 (2022). https://doi.org:10.1007/s13238-021-00882-3
25 Le Garff-Tavernier, M. *et al.* Human NK cells display major phenotypic and functional changes over the life span. *Aging Cell* **9**, 527-535 (2010). https://doi.org:10.1111/j.1474-9726.2010.00584.x
26 Almeida-Oliveira, A. *et al.* Age-related changes in natural killer cell receptors from childhood through old age. *Hum Immunol* **72**, 319-329 (2011). https://doi.org:10.1016/j.humimm.2011.01.009
27 Guo, C. *et al.* Single-cell transcriptomics reveal a unique memory-like NK cell subset that accumulates with ageing and correlates with disease severity in COVID-19. *Genome Med* **14**, 46 (2022). https://doi.org:10.1186/s13073-022-01049-3
28 Kurioka, A. *et al.* CD161 Defines a Functionally Distinct Subset of Pro-Inflammatory Natural Killer Cells. *Front Immunol* **9**, 486 (2018). https://doi.org:10.3389/fimmu.2018.00486
29 Schlums, H. *et al.* Cytomegalovirus infection drives adaptive epigenetic diversification of NK cells with altered signaling and effector function. *Immunity* **42**, 443-456 (2015). https://doi.org:10.1016/j.immuni.2015.02.008

Figure legends

Fig.1 Immune cell network of CBNB, Adults and elderly.

Immune cell network for each group was created where nodes are cellular subsets and edges are potential interaction between the subsets. Nodes are colour coded based on major immune cell lineage. Edges in green reflects negative correlation (inhibitory interaction) and red reflects positive interaction between the subsets. Thickness of the edges shows the strength of interaction (magnitude of correlation). A, B, C) Shows immune cell network of cord blood new born (CBNB), adults and elderly group respectively. D) Shows network property in a table format.

Fig.2 Association between Degree Centrality (DC) and frequency of immune cell subsets

A) Median frequency and DC of all immune cell subsets in CBNB, adult and elderly group was plotted as dot charts where each dot shows a node/subset. Blue line shows the linear regression line showing linear association between frequency and DC. Correlation coefficient (Pearson correlation) and P-value was also shown on each group plot. Median frequency and DC of selected node in B) CD4 T cell subsets C) CD8 T cell subset D) NK cell subsets were plotted as bar-plot. colour of the bars in bar-plot shows the human sample group information. Each node number is shown on Y -axis while median frequency and DC was shown on X-axis.

Fig.3 Degree Centrality (DC) and frequency of immune cell subsets from panel 2 dataset

Median frequency and DC of each node in A) Monocytes/DC cell subsets B) B cell subsets were plotted as bar-plot, colour of the bars in bar-plot shows the human sample group information. Each node number is shown on Y -axis while median frequency or DC was shown on X-axis.

Fig.4 Percentage of immune cell subsets observed in single cell transcriptomics data

Stacked bar-chart shows the cell counts for each subset observed in CBNB, adult and elderly group. Y- axis shows the cell types while X-axis shows cell counts (in thousands).

Fig.5. Ligand-Receptor interaction analysis corroborates the high degree centrality of CD161+NK cells

A) Figure shows the clusters of NK cell subsets on the t-SNE plot. B) group information was overlaid on t-SNE plots. C) Expression of KLRB1 gene (KLRB1 genes codes for CD161 protein) is overlaid on t-SNE plot. D) Figure shows the DC of the CD161+ and CD161- NK cell nodes from CyTOF data. E) LR interaction between NK cell cluster NK_0 (KLRB1+) and NK_3 (KLRB1-) similar to CyTOF Node 87 and Node 89 NK cell nodes shown as connected dot chart. The yellow dots represent the number of specific LR pairs enriched between NK_3 and other immune cell subsets shown on Y-axis and green dots denote LR pairs enriched between NK_0 and other immune cell subsets. The line connecting yellow and green dots indicates the difference in interaction potential of these NK cell subsets with other cell subsets.

Fig.6. Ligand-Receptor (LR) interaction explains exhaustion phenotype of CD28-CD8 T cells

A) Figure shows the clusters of CD8 T cells derived from scRNA seq overlaid on t-SNE plot. B) Cell type information predicted using MonocoData signature overlaid on t-SNE plot. C) group information was overlaid on t-SNE plots. D) Expression of CD28 gene overlaid on t-SNE plot. E) LR interaction between CD8_2 (CD28-CD8+) and CD8_1 (CD28+CD8+) and all other immune cell subsets from adults shown as connected dot chart. Yellow dots show the number of specific LR pairs enriched between CD8_2 (CD28-) and other immune cell subsets shown on Y-axis and green dots show LR pairs enriched between CD8_1(CD28+) and other immune cell subsets. F) LR interaction between CD8_0 (CD28-CD8+) and CD8_5 (CD28+CD8+) and all other immune cell subsets from CBNB were shown as a connected dot chart. Yellow dots show the number of specific LR pairs enriched between CD8_2/CD8_0 (CD28-) and other immune cell subsets shown on Y-axis and green dots show LR pairs enriched between CD8_1/CD8_5 (CD28+) and other immune cell subsets. The line connecting yellow and green dots indicates difference in interaction potential of these NK cell subsets with other cell subsets.

Extended data figure legends

Fig.S1 Phenotype of nodes (Immune cell subsets)

Normalised median antibody expression for all the nodes from A) Panel 1, and B) Panel 2 plotted as heatmap

Fig.S2 Degree Centrality (DC) and frequency of immune cell subsets from panel 1 dataset

Median frequency and DC of each node in A) CD4 T cell subsets C) CD8 T cell subset D) NK cell subsets were plotted as bar-plot. Colour of the bars in bar-plot shows the human sample group information. Each node number is shown on Y -axis while median frequency and DC was shown on X-axis.

Fig.S3 Interaction between the major lineage cell subsets.

Total number of edges between major cell lineage subsets in network of A) CBNB, B) Adult, C) Elderly were shown as a pie-chart and the number of edges between the subsets were listed in a table. Size of the pie in the circle reflects the fraction of edges normalised for total number of edges respective each network.

Fig.S4 Frequency of Major cell lineage in from CyTOF data.

Box and whisker plot showing frequencies of the major cell lineages (CD4 T cells, CD8 T cells, NK cells, Monocytes/DCs, B cells) in CBNB, adult and elderly groups.

Fig.S5 Directionality of Ligand-Receptor interaction analysis in NK cells

Ligand-Receptor **(**LR) interaction analysis shown separately for ligands signalling from A) NK cell subsets to other immune cell subsets or B) ligands signalling from other subsets to NK cell subsets. LR interactions between NK cell cluster NK_0 (KLRB1+) and NK_3 (KLRB1-) and other cell subsets were shown as a connected dot chart. Yellow dots show the number of specific LR pairs enriched between NK_3 and other immune cell subsets shown on Y-axis and green dots show LR pairs enriched between NK_0 and other immune cell subsets. Lines connecting yellow and green dots indicates the differences in interaction potential of these NK cell subsets with other cell subsets.

Supplementary Information

Supplementary Table S1: Human Subject demographic information

Supplementary Table S2: Cells counts of identified cell subsets in scRNA-seq data

Supplementary Table S3: Differential genes expressed in naive CD4T cells (CD4TN) compared to resting CD4 T cells (restCD4T)

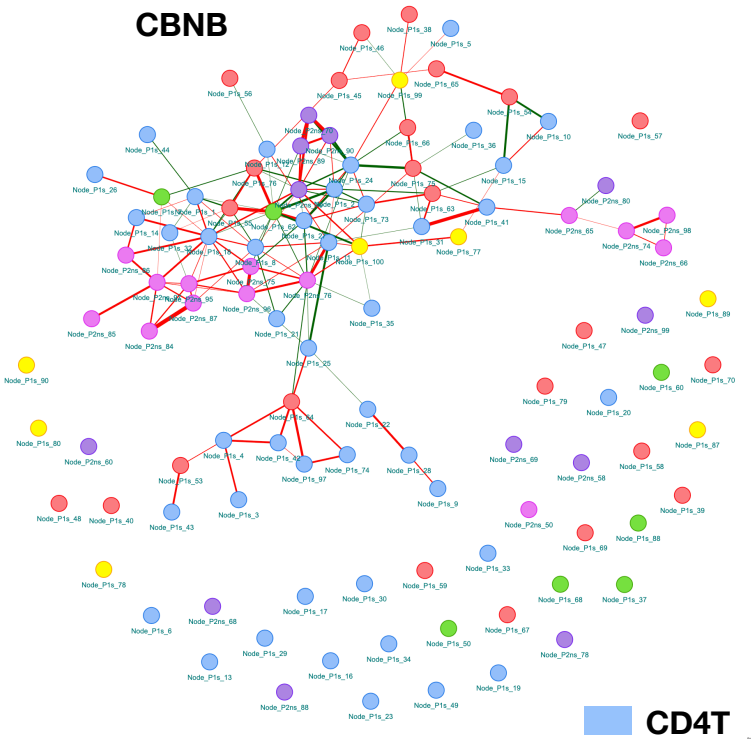

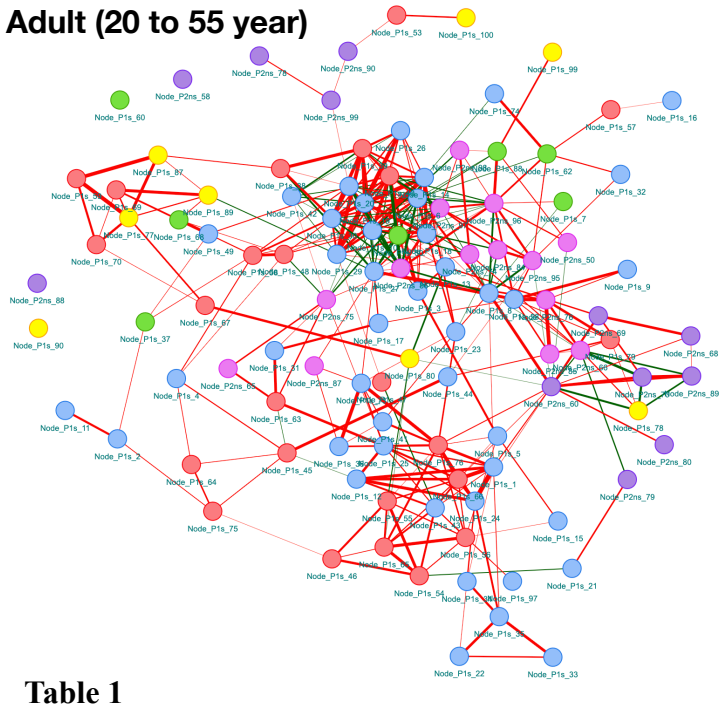

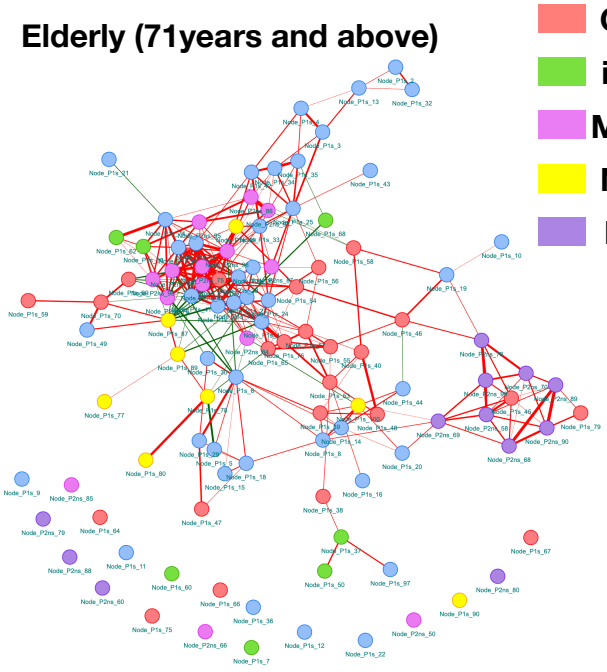

CD4T
CD8T
iT
Mo/DC
NK
Bcell

Table 1

Network property	CBNB	Adults	Elderly
edge/graph_density	0.02579	0.05798	0.05209
centralization_betweenness	0.07634	0.11214	0.09925
centralization_degree	0.10505	0.14763	0.15351
assortativity_degree	0.25068	0.35448	0.41068
diameter	10	9	10
average_path_length	3.77295	3.44044	3.56307
modularity	0.12948	0.14707	0.22729
no_neg_edges	56	73	38
no_pos_edges	93	262	263
Total edges	149	335	301
%neg	37.5%	21.7%	12.6%

Fig.1

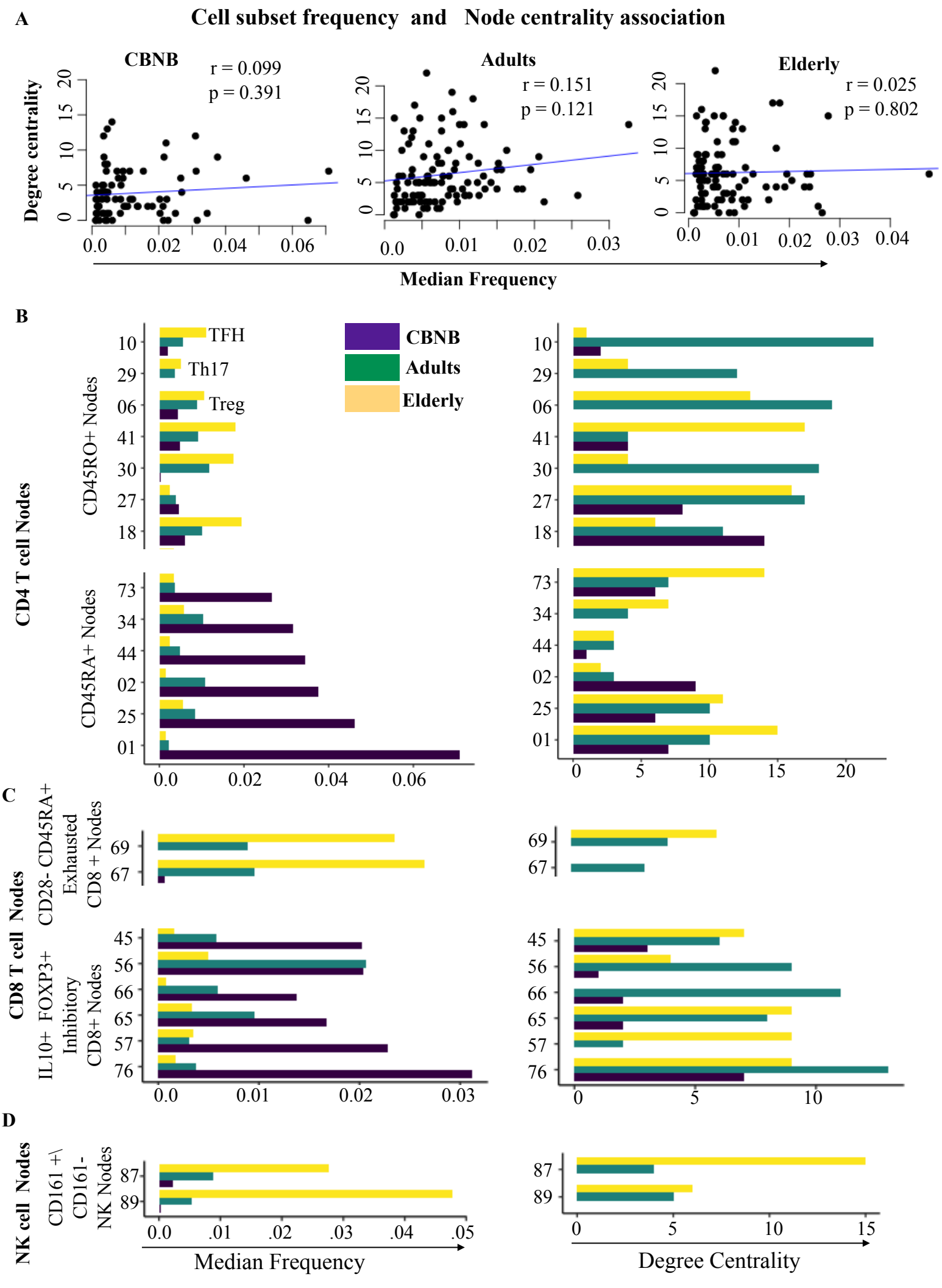
A
Cell subset frequency and Node centrality association
CBNB
r = 0.099
p = 0.391
Adults
r = 0.151
p = 0.121
Elderly
r = 0.025
p = 0.802
Degree centrality
Median Frequency
B
CD4 T cell Nodes
CD45RO+ Nodes
CD45RA+ Nodes
TFH
Th17
Treg
CBNB
Adults
Elderly
C
CD8 T cell Nodes
CD28- CD45RA+ Exhausted CD8 + Nodes
IL10+ FOXP3+ Inhibitory CD8+ Nodes
D
NK cell Nodes
CD161 +\ CD161- NK Nodes
Median Frequency
Degree Centrality

Fig.2

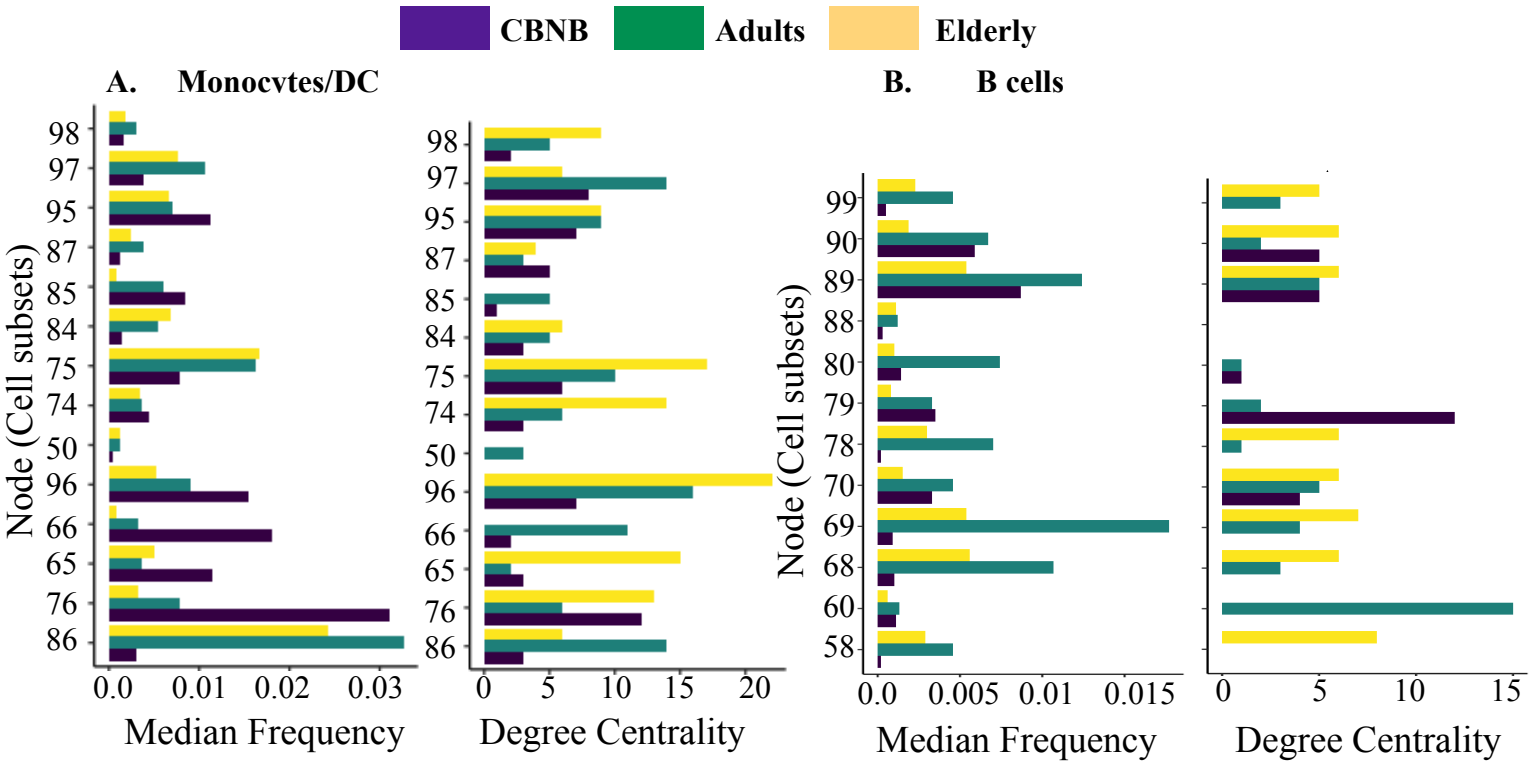
CBNB
Adults
Elderly
A. Monocytes/DC
B. B cells
Node (Cell subsets)
98
97
95
87
85
84
75
74
50
96
66
65
76
86
0.0
0.01
0.02
0.03
Median Frequency
0
5
10
15
20
Degree Centrality
99
90
89
88
80
79
78
70
69
68
60
58
0.0
0.005
0.01
0.015
Median Frequency
0
5
10
15
Degree Centrality

Fig.3

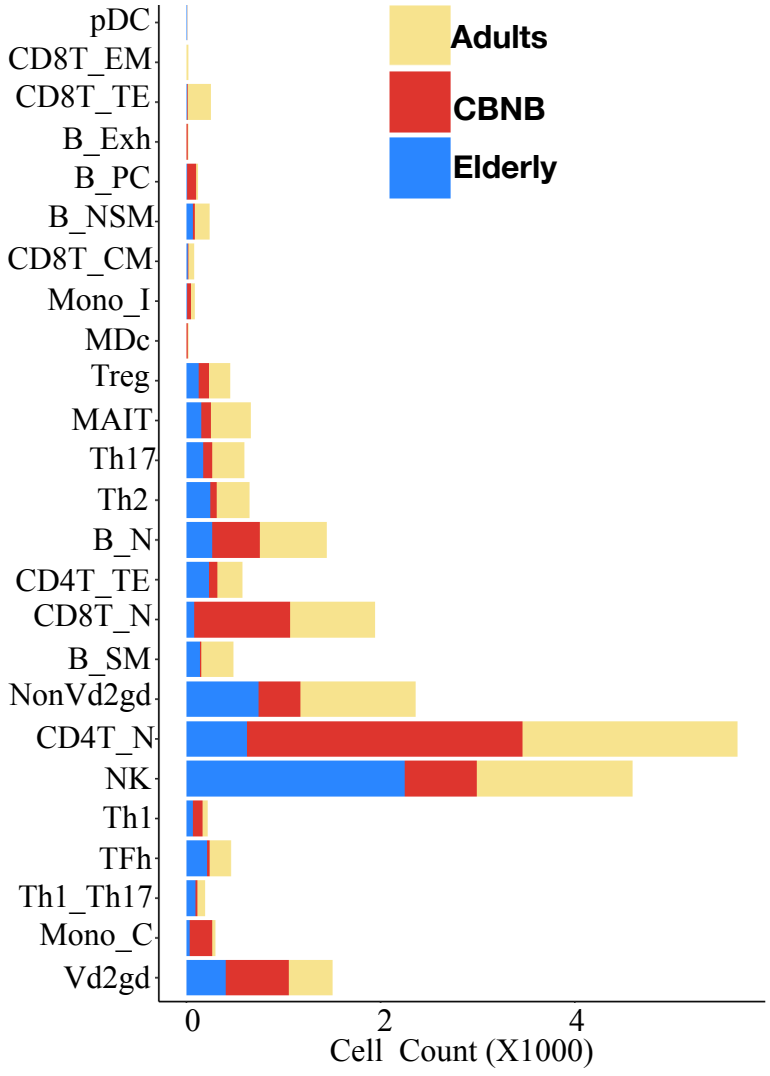
Adults
CBNB
Elderly
pDC
CD8T_EM
CD8T_TE
B_Exh
B_PC
B_NSM
CD8T_CM
Mono_I
MDc
Treg
MAIT
Th17
Th2
B_N
CD4T_TE
CD8T_N
B_SM
NonVd2gd
CD4T_N
NK
Th1
TFh
Th1_Th17
Mono_C
Vd2gd
0
2
4
Cell Count (X1000)

Fig.4

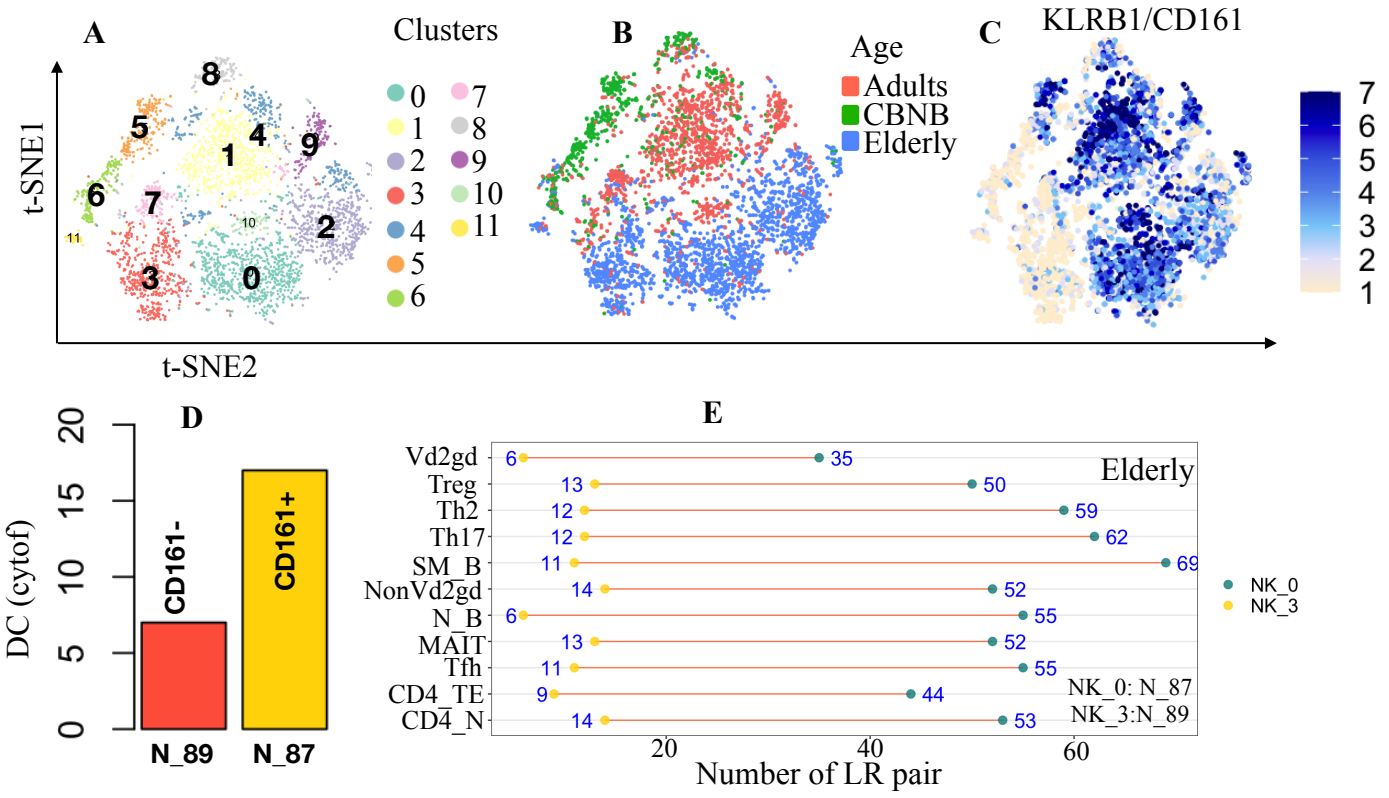
A
Clusters
0
1
2
3
4
5
6
7
8
9
10
11
t-SNE1
t-SNE2
B
Age
Adults
CBNB
Elderly
C
KLRB1/CD161
7
6
5
4
3
2
1
D
DC (cytof)
CD161-
CD161+
N_89
N_87
E
Elderly
Vd2gd
Treg
Th2
Th17
SM_B
NonVd2gd
N_B
MAIT
Tfh
CD4_TE
CD4_N
NK_0
NK_3
NK_0: N_87
NK_3:N_89
Number of LR pair

Fig.5

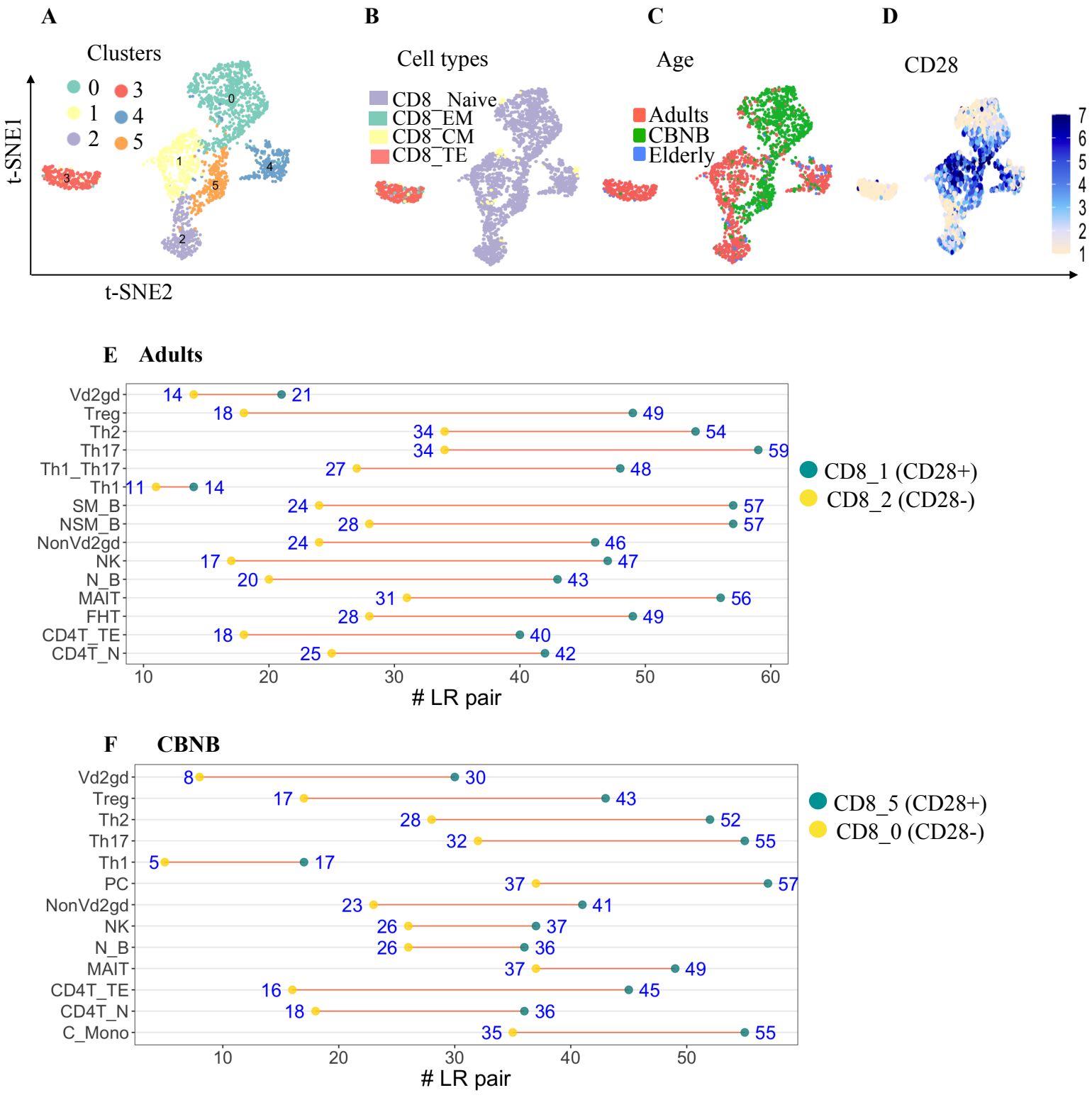
A
Clusters
0
1
2
3
4
5
B
Cell types
CD8_Naive
CD8_EM
CD8_CM
CD8_TE
C
Age
Adults
CBNB
Elderly
D
CD28
t-SNE1
t-SNE2
E Adults
Vd2gd
Treg
Th2
Th17
Th1_Th17
Th1
SM_B
NSM_B
NonVd2gd
NK
N_B
MAIT
FHT
CD4T_TE
CD4T_N
LR pair
CD8_1 (CD28+)
CD8_2 (CD28-)
F CBNB
Vd2gd
Treg
Th2
Th17
Th1
PC
NonVd2gd
NK
N_B
MAIT
CD4T_TE
CD4T_N
C_Mono
LR pair
CD8_5 (CD28+)
CD8_0 (CD28-)

Fig.6